Table A.1. Membership data for the open clusters.

DR2 SourceId	cluster	α (degr)	δ (degr)	ϖ_d mas	$\sigma\varpi_d$ mas
685747814353991296	Praesepe	133.15933	21.15502	5.645	0.033
685805259540481664	Praesepe	133.57003	21.73443	4.798	0.100
665141141087298688	Praesepe	130.22501	21.75663	5.630	0.020
...	...	...	...	...	...

Notes. Only the first three lines with data for members of the Praesepe cluster are presented here. For the more distant clusters, the last two columns are not included. The astrometric and photometric extra filters presented in Sect. 2.1 and used in the figures of this paper are not applied in this table. The full table will be available in electronic form at the CDS.

Appendix A: Open cluster membership and astrometric solutions

A.1. Nearby clusters

The nearby clusters were analysed with the method described and applied to the Hyades cluster in the first *Gaia* data release (Gaia Collaboration 2017). By combining the information from the measured proper motions and parallaxes for individual cluster members, it is possible to derive a higher precision measurement for the relative parallax of these cluster members. The proper motion observed for an individual cluster member represents the local projection on the sky of the baricentric velocity of the cluster. It is therefore affected by the angular separation on the sky of the member star from the projection of the cluster centre and the baricentric distance of the star, again relative to that of the cluster centre. Similarly, the measured parallax for the star can be significantly different from the mean parallax of the cluster.

The primary aim of the present paper is to provide high-precision HRDs, for which these accurate relative parallaxes contribute important information by reducing the actual differential distance modulus variations of cluster members. The effectiveness of this procedure is limited by the amplitude of the proper motion of the cluster centre and the ratio of the diameter over the distance of the cluster. The standard uncertainties in the individual parallaxes and proper motions of the cluster members in the second *Gaia* data release allow for this procedure to be applied for clusters within 250 pc. Table A.1 shows an example of an extract from the cluster member files produced for each of the nine clusters treated in this way.

Nine clusters within 250 pc from the Sun were analysed as nearby clusters. The analysis is iterative, and consists of two elements: 1. determinations of the space velocity vector at the cluster centre, and 2. determination of the cluster centre. A first selection is made of stars contained in a sphere with a radius of around 15 pc around the assumed centre of the cluster. A summary of the observed radii for the nearby and more distant clusters is shown in Fig. A.1. The radius can be adjusted based on the derived surface density distribution (Fig. A.2), where the outermost radius is set at the point beyond which the density of contaminating field stars starts to dominate. The selected stars are further filtered on their agreement between the observed proper motion and the predicted projection of the assumed space motion at the 3D position of the star, using the measured stellar parallax, and taking into account the uncertainties on the observed proper motion and parallax. The solution for the space motion follows Eq. A13 in Gaia Collaboration (2017). Although it is in principle possible to solve also for the radial velocity

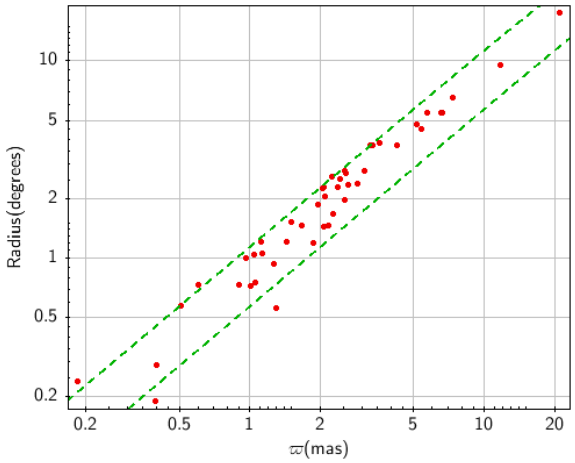

Fig. A.1. Maximum radius in degrees in DR2 for the 46 open clusters as a function of parallax. The two diagonal lines represent maximum radii of 10 (*bottom*) and 20 (*top*) pc.

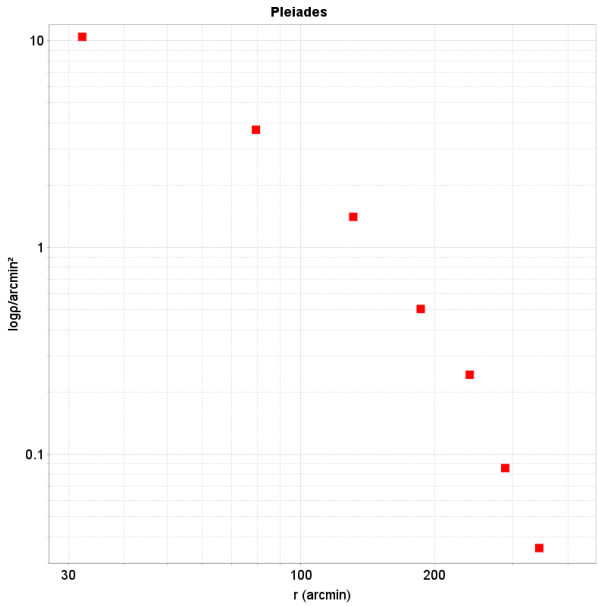

Fig. A.2. Surface-density profile for the Pleiades cluster, based on 1332 identified cluster members.

using only the astrometric data, this effectively only works for the Hyades cluster. Instead, a single equation for the observed radial velocity of the cluster was added, where the observed radial velocity is based on the weighted mean of the *Gaia* radial velocities of cluster members for which these data are available.

To stabilise the solution, it is important to align the coordinate system with the line of sight towards the cluster centre, minimising the mixing of the contributions from the proper motions and the additional information from the radial velocity. The solution for the space motion does provide an estimate of the radial velocity component, but except for the Hyades and Coma Ber, this is largely dominated by the radial velocity value and its accuracy that is used as input to the solution. Small differences are therefore seen between the radial velocities as presented in Table A.2 (as directly derived from the *Gaia* spectroscopic data) and in Table A.3 (the summary data for the nine clusters in this selection), where the astrometric information on the radial velocity is also taken into account. Figure A.3 shows an example of the level of agreement between the differential

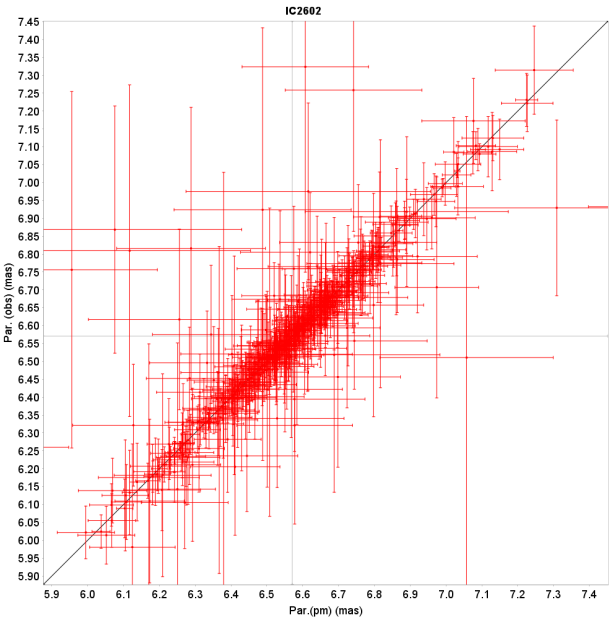

Fig. A.3. Comparison between the directly measured parallaxes and the parallaxes obtained by including the relative proper motion data, for the cluster IC 2602. The clear linear relation shows the good agreement between proper motion and parallax offsets from the mean cluster values.

Table A.2. Mean radial velocity values as derived from the *Gaia* spectroscopic data for nearby clusters.

Name	$V_{\rm rad}$	$\sigma(V_{\rm rad})$	uwsd	Nobs
Hyades	39.87	0.05	2.28	150
ComaBer	0.21	0.13	2.15	43
Pleiades	5.54	0.10	2.00	195
IC2391	15.00	0.24	1.19	35
IC2602	17.62	0.22	1.24	36
alphaPer	−0.32	0.17	1.38	71
Praesepe	34.84	0.07	1.45	176
NGC2451A	23.08	0.34	1.32	31
Blanco1	6.01	0.15	1.03	51

Notes. Columns: 1. Cluster name; 2: weighted-mean radial velocity in km s^{-1}; 3. standard uncertainty on radial velocity; 4. unit-weight standard deviation of mean velocity solution; and 5. number of observations in mean velocity solution.

parallax and proper motion values in the cluster IC 2602. In Fig. A.4 we also show an example of the 3D distribution maps for this cluster; maps like this were prepared for all nearby clusters.

Next to the astrometric data, the second *Gaia* data release also presents radial velocity measurements for a magnitude-limited sample. The radial velocities were compared with the projection of the cluster space velocity at the position of each star for which these data are available. This is particularly relevant for stars in the Hyades cluster, where the projection effects of the radial velocity can be of the order of several km s^{-1}. Table A.2 presents the results for the nine nearby clusters.

Figure A.5 shows the differences (observed − predicted, where the predicted value is based on the local projection of the space velocity of the cluster) in the radial velocities for 191 stars in the Hyades cluster. Only stars for which the colour index $G_{\rm BP} - G_{\rm RP}$ is greater than 0.4 mag were used. The results for all 9 nearby clusters are shown in Table A.2.

A.2. More distant open clusters

For the more distant clusters, a selection was made of 37 relatively rich clusters, generally only little reddened, and as far as possible, covering a spread in ages and chemical composition (Fig. A.6). These clusters were all analysed in a combined solution of the mean parallax and proper motion from the observed astrometric data of the member stars. This is an iterative procedure, where cluster membership determination is based on the solution for the astrometric parameters of the cluster. The combined solution for the astrometric parameters of a cluster takes into account noise contributions from three sources:

1. the covariance matrix of the astrometric solution for each star;
2. the internal velocity dispersion of the cluster, affecting the dispersion of the proper motions;
3. the effect of the cluster size relative to its distance, which
   (a) is reflected in a dispersion on the parallaxes of the cluster members;
   (b) is reflected in a dispersion in proper motions in the direction of, and scaled by, the cluster proper motion.

When we assume that the velocity distribution is isotropic within the measurement accuracy, then the second of these noise contributions will be diagonal. The first and third may also contain significant off-diagonal elements. Given a cluster parallax of ϖ_c, a cluster proper motion of $(\mu_{\alpha,c}, \mu_{\delta,c})$, and an average relative dispersion in the parallaxes of the cluster stars of $\sigma_\varpi/\varpi = \sigma_R/R$ (where R is the distance to the cluster centre), the contribution to the dispersion in the proper motions of the cluster stars scales with the relative dispersion of the parallaxes and the proper motions of the cluster:

$$\sigma\mu_{\alpha,s} = |\mu_{\alpha,c}| \times \sigma_\varpi/\varpi \quad \text{(A.1)}$$

$$\sigma\mu_{\delta,s} = |\mu_{\delta,c}| \times \sigma_\varpi/\varpi. \quad \text{(A.2)}$$

For most of the clusters with distances beyond 250 pc, this contribution will be small to very small relative to other contributions. Figure A.7 shows the overall relation between parallaxe and proper motion amplitudes for the selection of clusters we used.

The contributions are summed into a single noise matrix, of which an upper-triangular square root is used to normalise the observation equations that describe the cluster proper motion and parallax as a function of the observed proper motions and parallaxes of the individual cluster members.

Table A.4 presents an overview of the astrometric solutions for 37 open clusters, with mean radial velocities when available in the *Gaia* data. We note that some clusters are not included in Table 2 because their colour-magnitude diagrams are too disturbed by interstellar extinction (see an illustration of the differential extinction effect in Fig. A.8). The proper motions are compared with those presented by Loktin & Beshenov (2003) in Fig. A.9, and they agree well overall, but there is also an indication that errors on the data presented in Loktin & Beshenov (2003) are underestimated. In the same figure the comparison between the parallaxes as derived from the DR2 data and parallax values derived from photometric distances as (mostly) presented in Kharchenko et al. (2005) are shown, and again generally agree well (see also the validation with more clusters in Arenou et al. 2018). The systematic difference of 0.029 mas, which can be observed for globular clusters (Gaia Collaboration 2018c), is too small to be noticed here (Fig. A.10), but the calibration noise on the DR2 parallaxes (0.025 mas), obtained in the same study, is significantly larger than the standard uncertainties

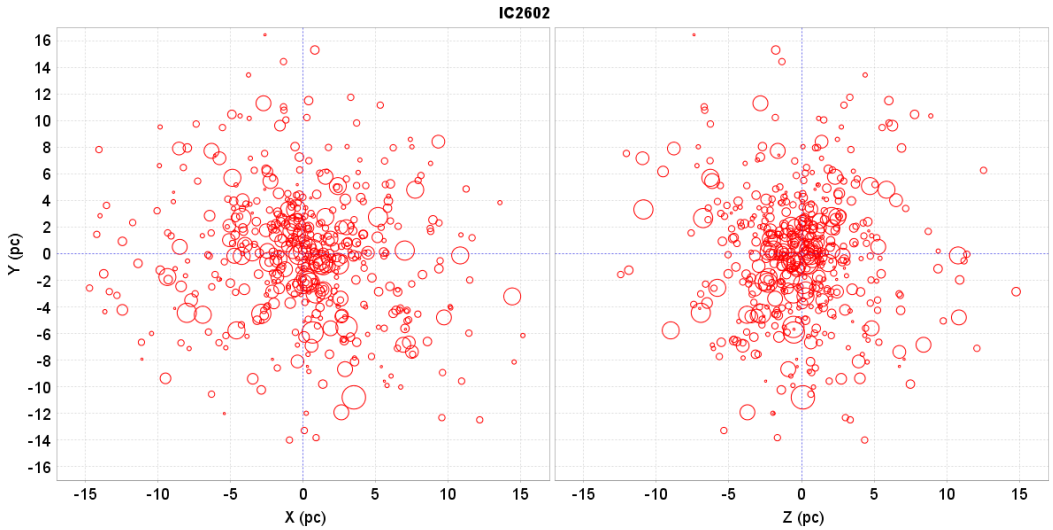

Fig. A.4. Distribution of stars in IC 2602 in galactic rectangular coordinates, showing the flattening in the Z (galactic pole) direction.

Table A.3. Space velocity fitting results for nearby clusters.

Name ClustId	U' σU' km/s	V' σV' km/s	W' σW' km/s	$c_{U'V'}$ $c_{V'W'}$	$c_{U'W'}$ σv	uwsd Observ.	α_c δ_c degr.	ϖ $\sigma\varpi$ mas	V_{rad} σV_{rad} km/s	$\mu_{\alpha*}$ $\sigma\mu_{\alpha*}$ mas/yr	μ_δ $\sigma\mu_\delta$ mas/yr
Hyades	−6.059	45.691	5.544	0.33	0.35	0.67	97.5407	21.052	39.96	101.005	−28.490
C0424+157	0.031	0.069	0.025	0.93	0.40	515	6.8148	0.065	0.06	0.171	0.137
ComaBer	−1.638	4.785	−3.528	0.35	−0.86	0.48	110.1896	11.640	−0.52	−12.111	−8.996
C1222+263	0.078	0.018	0.040	−0.39	0.40	153	−34.3206	0.034	0.07	0.048	0.121
Pleiades	−1.311	21.390	−24.457	0.48	0.50	0.77	93.5183	7.364	5.65	19.997	−45.548
C0344+239	0.070	0.105	0.057	0.90	0.40	1326	−48.7831	0.005	0.09	0.127	0.101
Praesepe	0.339	49.097	1.200	−0.50	−0.60	0.76	89.5122	5.371	35.64	−36.047	−12.917
C0937+201	0.090	0.106	0.050	0.92	0.40	938	1.3517	0.003	0.10	0.110	0.066
alphaPer	−5.110	24.183	−14.122	0.25	0.40	0.68	101.9183	5.718	−0.29	22.929	−25.556
C0318+484	0.053	0.067	0.097	0.59	0.40	740	−29.7555	0.005	0.08	0.071	0.095
IC2391	−0.751	28.459	−1.590	−0.20	0.38	0.68	91.6471	6.597	14.59	−24.927	23.256
C0838-528	0.054	0.062	0.105	−0.52	0.40	325	−3.4126	0.007	0.09	0.080	0.110
IC2602	−9.467	16.867	−12.377	−0.05	0.40	0.72	119.3285	6.571	17.43	−17.783	10.655
C1041-641	0.056	0.024	0.120	−0.16	0.40	492	−32.7371	0.007	0.11	0.040	0.098
Blanco1	6.176	21.150	−0.296	0.01	−0.86	0.65	73.6042	4.216	5.78	18.724	2.650
C0001-302	0.111	0.020	0.065	−0.02	0.40	489	−0.8388	0.003	0.10	0.017	0.070
NGC2451	5.806	32.440	−3.100	−0.24	0.34	0.68	79.8905	5.163	22.85	−21.063	15.378
C0743-378	0.048	0.095	0.084	−0.76	0.40	400	−5.4202	0.005	0.09	0.065	0.093

Notes. Columns: 1. Cluster identifiers; 2 to 4 U', V' and W' velocity components in the equatorial system; 5. U'V' error correlation (top) V'W' error correlation (bottom); 6. U'W' error correlation (top), applied internal velocity dispersion in km s^{-1} (bottom); 7. unit-weight standard deviation of solution (top), number of stars (bottom); 8. Coordinates of the convergent point; 9. parallax (mas); 10. radial velocity (km s^{-1}); 11. proper motion in right ascension; and 12. proper motion in declination.

on the mean cluster parallaxes and is therefore the main contributor to the uncertainties on the cluster parallaxes. In most cases, however, this amounts to less than 1% in error on the parallax, or 0.02 mag in distance modulus.

The maximum radius for each cluster was determined from the contrast between the cluster and the field stars in the proper motion and parallax domain. In practice, this means that the density of field stars for which the combined information on the parallax and proper motion, combined with uncertainties and error correlations, leaves a significant possibility for a field star to be a cluster member. When the surface density of these field stars becomes similar to the surface density of the cluster stars, we have reached the maximum radius for the cluster in this particular data set and parameter space. It is well possible, however, that for a catalogue with higher accuracies on the astrometric parameters for the fainter stars in particular, this limit will be found still farther away from the cluster centre. Radial velocities for the clusters, mostly as given in Kharchenko et al. (2005) or Conrad et al. (2014), were compared with the mean radial velocities as derived from the *Gaia* DR2 data. A limited spectral range was used, for which there is clear consistency of the radial velocity measurements. The summary of the results is shown in Fig. A.9 and generally agrees well (see also the validation with more clusters in Arenou et al. 2018). The largest discrepancies are found for NGC 2516 (RAVE measurements in Conrad et al. 2014) and Trumpler 2 (Kharchenko et al. 2005).

Table A.4. Overview of the results for open clusters with distances beyond 250 pc

Name ClustId	α δ deg	ϖ σ_ϖ mas	$\mu_{\alpha*}$ $\sigma_{\mu\alpha*}$ mas/yr	μ_δ $\sigma_{\mu\delta}$ mas/yr	c_{12} c_{13}	c_{23} r(max)$^\circ$	nMemb st.dev.	Vrad σ km s^{-1}	uwsd Obs.
NGC0188	11.7494	0.5053	−2.3087	−0.9565	−0.04	−0.02	1181	−41.86	1.43
C0039+850	85.2395	0.0011	0.0035	0.0030	0.16	0.58	0.84	0.13	20
NGC0752	29.2054	2.2304	9.8092	−11.7637	0.02	−0.04	433	5.90	1.68
C0154+374	37.7454	0.0027	0.0191	0.0180	0.04	2.58	0.86	0.11	76
Stock2	33.8282	2.6367	15.8241	−13.7669	0.01	0.01	1742	8.58	1.45
C0211+590	59.5813	0.0009	0.0103	0.0104	−0.00	2.36	0.78	0.09	109
NGC0869	34.7391	0.3942	−0.6943	−1.0831	0.14	0.10	829		
C0215+569	57.1339	0.0014	0.0038	0.0041	0.08	0.19	0.83		0
NGC0884	35.5430	0.3976	−0.6021	−1.0616	0.16	0.11	1077	−44.69	4.98
C0218+568	57.1591	0.0012	0.0035	0.0036	0.10	0.29	0.86	0.73	2
Trump02	39.1879	1.4316	1.5305	−5.3361	0.05	0.04	589	−4.06	0.75
C0233+557	55.8846	0.0023	0.0116	0.0117	0.01	1.21	0.90	0.09	4
NGC1039	40.5843	1.9536	0.7256	−5.7320	0.02	−0.02	764	−7.27	1.44
C0238+425	42.7027	0.0027	0.0109	0.0103	0.04	1.87	0.79	0.72	18
NGC1901	79.6838	2.3582	1.5953	12.6920	0.03	0.10	290	1.62	1.60
C0518-685	−68.1627	0.0031	0.0276	0.0277	−0.03	2.30	1.04	0.56	16
NGC2158	91.8751	0.1833	−0.1665	−1.9932	0.18	−0.19	3942	26.64	2.30
C0604+241	24.1163	0.0021	0.0035	0.0029	0.21	0.24	0.92	0.60	11
NGC2168	92.2688	1.1301	2.2784	−2.9336	0.08	−0.08	1794	−7.70	2.73
C0605+243	24.3148	0.0013	0.0052	0.0050	0.05	1.20	0.87	0.27	6
NGC2232	96.9973	3.0710	−4.7737	−1.9014	0.04	−0.04	318	24.22	0.96
C0624-047	−4.7929	0.0033	0.0185	0.0181	0.04	2.76	0.78	0.44	9
Trump10	131.8982	2.2637	−12.3536	6.5309	0.02	0.00	947	21.97	1.00
C0646-423	−42.5192	0.0014	0.0102	0.0104	−0.01	1.69	0.82	0.31	28
NGC2323	105.7245	1.0012	−0.7977	−0.6540	0.06	−0.03	382	11.55	
C0700-082	−8.3586	0.0017	0.0063	0.0063	0.00	0.73	0.87		1
NGC2360	109.4452	0.9018	0.3853	5.5893	0.07	−0.02	1037	28.02	1.74
C0715-155	−15.6317	0.0012	0.0048	0.0048	−0.05	0.74	0.79	0.19	15
Coll140	111.0308	2.5685	−8.1285	4.7105	0.02	0.02	332	18.53	1.75
C0722-321	−32.1113	0.0025	0.0215	0.0220	−0.01	2.69	0.81	1.85	5
NGC2423	114.2904	1.0438	−0.7343	−3.6333	0.09	−0.00	694	18.50	2.04
C0734-137	−13.8348	0.0017	0.0070	0.0069	−0.04	1.04	0.81	0.17	19
NGC2422	114.1463	2.0690	−7.0200	0.9592	0.05	0.01	907	36.21	1.42
C0734-143	−14.4844	0.0014	0.0098	0.0099	−0.02	1.45	0.74	0.57	30
NGC2437	115.4358	0.6005	−3.8232	0.3729	0.11	0.01	3032	37.34	
C0739-147	−14.8506	0.0009	0.0031	0.0031	−0.06	0.74	0.83		1
NGC2447	116.1262	0.9603	−3.5680	5.0434	0.03	0.01	926	22.37	3.01
C0742-237	−23.8567	0.0013	0.0056	0.0057	−0.01	1.00	0.80	0.26	11
NGC2516	119.5469	2.4118	−4.6579	11.1517	0.02	−0.00	2518	23.78	1.39
C0757-607	−60.7749	0.0006	0.0075	0.0075	−0.01	2.54	0.83	0.11	156
NGC2547	122.5654	2.5438	−8.5999	4.2542	0.02	0.00	644	15.46	2.47
C0809-491	−49.0498	0.0015	0.0148	0.0148	−0.00	2.79	0.78	0.83	22
NGC2548	123.3834	1.2897	−1.3302	1.0164	0.13	0.00	509	8.83	1.77
C0811-056	−5.7363	0.0024	0.0095	0.0093	−0.03	0.56	0.80	0.27	8
NGC2682	132.8476	1.1325	−10.9737	−2.9396	0.08	−0.00	1520	34.05	1.94
C0847+120	11.8369	0.0011	0.0064	0.0063	−0.01	1.06	0.76	0.10	66
NGC3228	155.3791	2.0323	−14.8800	−0.6498	0.03	0.03	222		
C1019-514	−51.7693	0.0029	0.0220	0.0220	−0.01	2.27	0.81		0
NGC3532	166.3975	2.0659	−10.3790	5.1958	0.03	−0.02	1879	4.85	2.24
C1104-584	−58.7335	0.0007	0.0079	0.0079	0.01	2.31	0.79	0.13	143
NGC6025	240.7714	1.2646	−2.8846	−3.0222	−0.02	0.01	452	−7.66	
C1559-603	−60.4562	0.0015	0.0100	0.0099	0.03	0.94	0.75		1
NGC6281	256.1638	1.8716	−1.8764	−3.9506	−0.03	0.05	573	−5.02	2.17
C1701-378	−37.9180	0.0019	0.0144	0.0136	0.05	1.19	0.80	0.20	21
IC4651	261.2035	1.0542	−2.4051	−5.0280	−0.07	0.10	960	−30.32	3.41
C1720-499	−49.9185	0.0014	0.0061	0.0060	0.06	0.76	0.80	0.19	56
NGC6405	265.1220	2.1626	−1.3662	−5.8063	−0.04	0.11	967	−9.20	5.39

Table A.4. continued.

Name ClustId	α δ deg	ϖ σ_ϖ mas	$\mu_{\alpha*}$ $\sigma_{\mu\alpha*}$ mas/yr	μ_δ $\sigma_{\mu\delta}$ mas/yr	c_{12} c_{13}	c_{23} r(max)°	nMemb st.dev.	Vrad σ km s^{-1}	uwsd Obs.
C1736-321	−32.4135	0.0021	0.0140	0.0132	0.04	1.46	0.82	0.77	17
IC4665	266.4978	2.8918	−0.8993	−8.5114	−0.02	0.04	174	−11.26	1.86
C1743+057	5.5653	0.0034	0.0347	0.0345	0.02	2.39	0.75	2.12	6
NGC6475	268.2736	3.5704	3.0722	−5.3157	−0.02	0.04	1140	−14.84	2.63
C1750-348	−34.6639	0.0016	0.0185	0.0184	0.02	3.86	0.82	0.17	113
NGC6633	276.8737	2.5232	1.1584	−1.7371	−0.03	0.09	321	−28.59	1.83
C1825+065	6.6081	0.0023	0.0199	0.0200	0.01	1.99	0.84	0.14	28
IC4725	277.9462	1.5043	−1.7201	−6.1010	−0.07	0.09	755		
C1828-192	−19.1058	0.0019	0.0091	0.0091	0.04	1.53	0.89		0
IC4756	279.6698	2.0943	1.2574	−4.9145	−0.04	0.06	543	−24.72	2.76
C1836+054	5.3836	0.0018	0.0134	0.0134	0.02	2.05	0.84	0.17	38
NGC6774	289.1055	3.2516	−0.9733	−26.6464	−0.03	0.11	234	41.79	3.36
C1913-163	−16.3901	0.0038	0.0367	0.0383	0.00	3.74	1.00	0.15	62
NGC6793	290.7795	1.6672	3.8120	3.5622	−0.03	0.06	465	−10.85	
C1921+220	22.1400	0.0021	0.0131	0.0136	−0.02	1.47	0.81		1
NGC7092	322.4220	3.3373	−7.3569	−19.5993	−0.02	−0.00	433	−5.07	0.95
C2130+482	48.1315	0.0024	0.0256	0.0260	−0.00	3.72	0.86	0.21	21

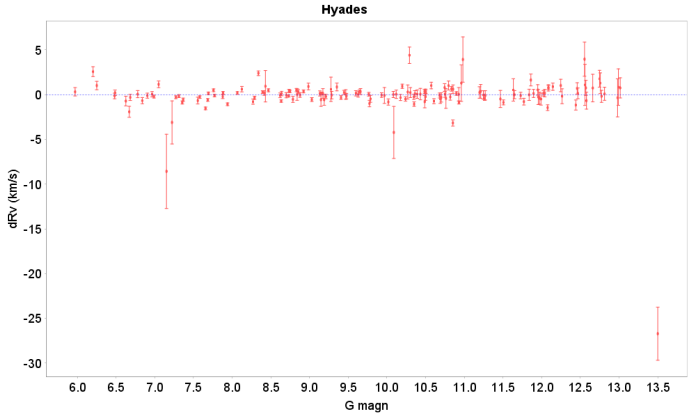

Fig. A.5. Differences between the predicted and observed radial velocities in the Hyades cluster as a function of G magnitude.

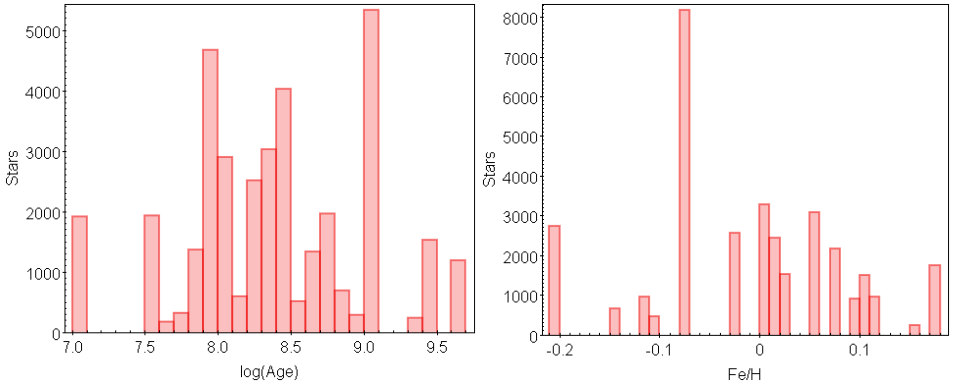

Fig. A.6. Distributions over age and composition for stars in the 32 open clusters selected for the composite HRD, including the nearby clusters.

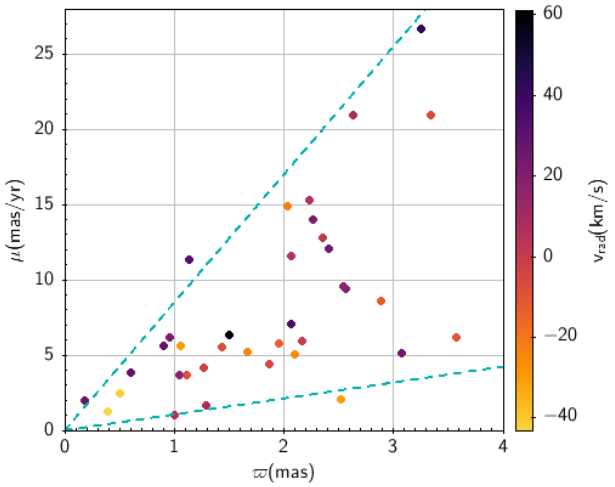

Fig. A.7. Comparison between the parallaxes and proper motions for the 37 open clusters. The upper and lower diagonal lines represent tangential velocities of 40 and 5 km s^{-1} , respectively.

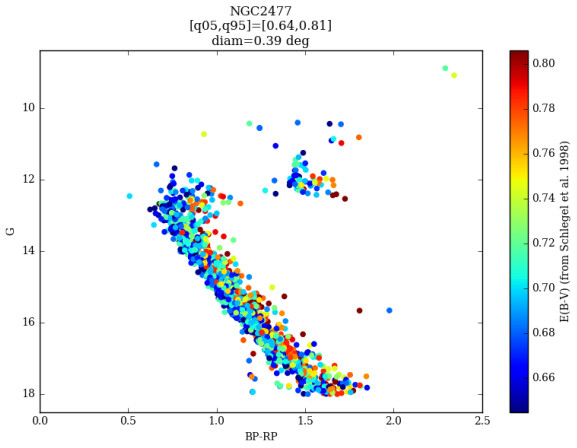

Fig. A.8. Colour-magnitude diagram of NGC 2477, with each star colour-coded by the value of integrated extinction in the catalogue of Schlegel et al. (1998).

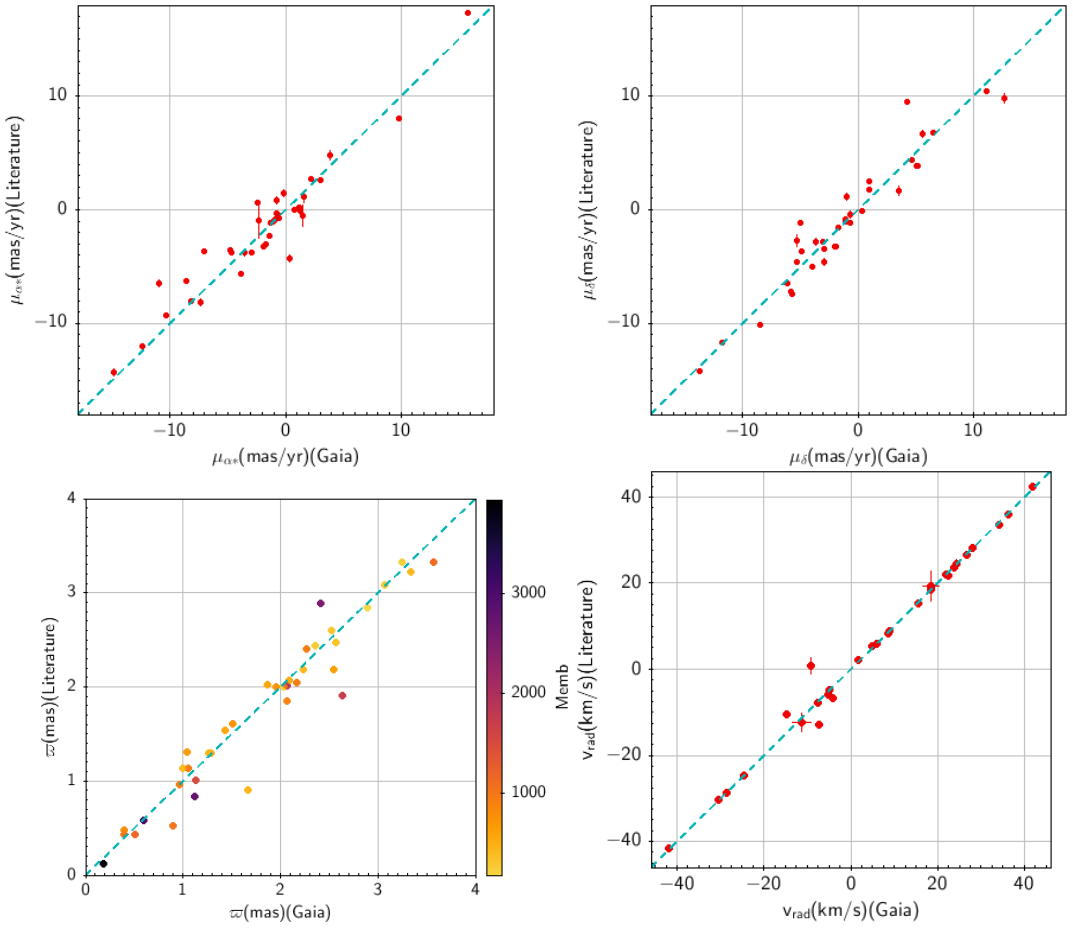

Fig. A.9. Comparisons with values quoted in literature (see text) for (*top*) proper motions in right ascension, proper motions in declination, (*bottom*) parallaxes, and radial velocities for 37 open clusters with distances beyond 250 pc.

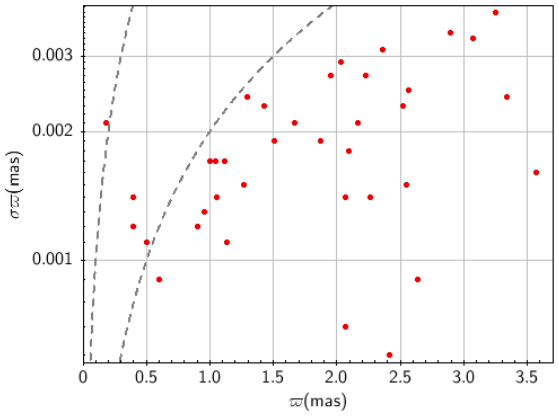

Fig. A.10. Standard uncertainties on the mean cluster parallax determinations. The curves represent the 100 and 500 σ significance levels when only the standard uncertainties are considered.

Appendix B: *Gaia* archive query

The *Gaia* archive[6] query corresponding to the filters described in Sect. 2.1 is the following (selecting here the first five stars):

```
SELECT TOP 5 phot_g_mean_mag+5*log10(parallax)-10 AS mg, bp_rp FROM gaiadr2.gaia_source
   WHERE parallax_over_error > 10
   AND phot_g_mean_flux_over_error>50
   AND phot_rp_mean_flux_over_error>20
   AND phot_bp_mean_flux_over_error>20
   AND phot_bp_rp_excess_factor < 1.3+0.06*power(phot_bp_mean_mag-phot_rp_mean_mag,2)
   AND phot_bp_rp_excess_factor > 1.0+0.015*power(phot_bp_mean_mag-phot_rp_mean_mag,2)
   AND visibility_periods_used>8
   AND astrometric_chi2_al/(astrometric_n_good_obs_al-5)<1.44*greatest(1,exp(-0.4*(phot_g_mean_mag-19.5)))
```

[6] https://gea.esac.esa.int/archive/